Eur J Nucl Med Mol Imaging (2009) 36:53–62
DOI 10.1007/s00259-008-0891-1

ORIGINAL ARTICLE

MicroPET imaging of 5-HT_{1A} receptors in rat brain: a test–retest [^{18}F]MPPF study

Nicolas Aznavour · Chawki Benkelfat · Paul Gravel · Antonio Aliaga · Pedro Rosa-Neto · Barry Bedell · Luc Zimmer · Laurent Descarries

Received: 9 May 2008 / Accepted: 11 July 2008 / Published online: 15 August 2008

Abstract
Purpose Earlier studies have shown that positron emission tomography (PET) imaging with the radioligand [^{18}F]MPPF allows for measuring the binding potential of serotonin 5-hydroxytryptamine$_{1A}$ (5-HT_{1A}) receptors in different regions of animal and human brain, including that of 5-HT_{1A} autoreceptors in the raphe nuclei. In the present study, we sought to determine if such data could be obtained in rat, with a microPET (R4, Concorde Microsystems).
Methods Scans from isoflurane-anaesthetised rats (n=18, including six test–retest) were co-registered with magnetic resonance imaging data, and binding potential, blood to plasma ratio and radiotracer efflux were estimated according to a simplified reference tissue model.
Results Values of binding potential for hippocampus (1.2), entorhinal cortex (1.1), septum (1.1), medial prefrontal cortex (1.0), amygdala (0.8), raphe nuclei (0.6), paraventricular hypothalamic nucleus (0.5) and raphe obscurus (0.5) were comparable to those previously measured with PET in cats, non-human primates or humans. Test–retest variability was in the order of 10% in the larger brain regions (hippocampus, medial prefrontal and entorhinal cortex) and less than 20% in small nuclei such as the septum and the paraventricular hypothalamic, basolateral amygdaloid and raphe nuclei.
Conclusions MicroPET brain imaging of 5-HT_{1A} receptors with [^{18}F]MPPF thus represents a promising avenue for investigating 5-HT_{1A} receptor function in rat.

N. Aznavour · C. Benkelfat · P. Gravel
Department of Psychiatry, McGill University,
Montreal, QC, Canada

C. Benkelfat · P. Gravel · B. Bedell
Department of Neurology and Neurosurgery, McGill University,
Montreal, QC, Canada

A. Aliaga · B. Bedell
Department of Small Animal Imaging Laboratory,
McGill University,
Montreal, QC, Canada

P. Rosa-Neto
Molecular NeuroImaging Laboratory, Douglas Hospital,
Montreal, QC, Canada

L. Zimmer
ANIMAGE Department, CERMEP,
Lyon, France

L. Zimmer
Université Lyon 1 and CNRS,
Lyon, France

L. Descarries
Department of Pathology and Cell Biology,
Université de Montréal,
Montreal, QC, Canada

L. Descarries
Department of Physiology,
Université de Montréal,
Montreal, QC, Canada

L. Descarries
GRSNC, Université de Montréal,
Montreal, QC, Canada

N. Aznavour (✉)
EPFL, SV, BMI,
Laboratory of Neuroenergetics and Cellular Dynamics,
AAB 2 01 (Bâtiment AAB), Station 15,
CH-1015 Lausanne, Switzerland
e-mail: nicolas.aznavour@epfl.ch

Keywords Binding potential · Serotonin receptors · Brain imaging · Autoreceptors · Positron emission tomography

Introduction

The brain serotonin [5-hydroxytryptamine (5-HT)] system regulates a variety of functions and behaviours (reviewed in [1, 2]) via a neuronal network pervading most regions of the neuraxis [3–8] and operating through at least 14 5-HT receptor subtypes [9]. Particular attention has been paid to the characterisation of the structural, pharmacological and functional properties of the serotonin$_{1A}$ receptors (5-HT$_{1A}$R; e.g. [10]) owing to their implication in different neurological and psychiatric diseases [11] and their established role in the action of antidepressants/anxiolytics, such as the selective serotonin reuptake inhibitors (reviewed in [12]). 5-HT$_{1A}$R act as autoreceptors on the soma and dendrites of 5-HT neurons themselves, in the raphe dorsalis nucleus (RN), for example, and as somatodendritic (so-called post-synaptic) heteroreceptors in territories of 5-HT projection, such as hippocampus and cerebral cortex. Because 5-HT$_{!A}$ autoreceptors negatively control the firing and release of 5-HT neurons (reviewed in [13]), their desensitisation, together with increased sensitivity and signalling of 5-HT$_{1A}$ heteroreceptors [14–18], is generally viewed as accounting for the increases in 5-HT neurotransmission underlying the efficacy of antidepressant treatments.

Several ligands have been developed to image 5-HT$_{1A}$R in vivo with positron emission tomography (PET), among which the selective 5-HT$_{1A}$ receptor antagonist, 4-2′-(methoxyphenyl)-1-[2″-(*N*-2″-pyridinyl)-*p*-fluorobenzamido] ethyl-piperazine (MPPF), labelled with [^{18}F]fluorine: [^{18}F] MPPF [19, 20]. Preliminary radiopharmacological experiments have indicated that the regional distribution of [^{18}F] MPPF in rat brain matches the density of 5-HT$_{1A}$R binding sites [21, 22]. [^{18}F]MPPF has been successfully used for PET studies in cat, monkey and human brain (reviewed in [23]).

An initial microPET study with [^{18}F]MPPF has already shown high binding of this radioligand in the hippocampus of anaesthetised rat [21]. [^{18}F]MPPF microPET imaging is of particular interest in this species, in view of the detailed knowledge of its 5-HT system and the increasing use of rodent models for investigating a variety of pathological conditions and their treatment, including mood disorders. Moreover, combined immuno-electron microscopic studies of 5-HT$_{1A}$R and β-microprobe measurement of the in vivo binding of [^{18}F]MPPF in rat have shown that after acute treatment with the prototypical SSRI, fluoxetine (Prozac), selective decreases in [^{18}F]MPPF binding are associated with 5-HT$_{1A}$ autoreceptor internalisation in the dorsal raphe nucleus [24, 25]. Moreover, under similar conditions, decreases in binding potential (BP) have been measured with PET in the dorsal raphe nucleus of cat and human [26, 27]. From a brain imaging perspective, PET scanners designed to image small animals offer the advantage of having better spatial resolution (<1.85 mm) than full-size PET scanners (4 mm) but lower sensitivity. In this context, it was deemed useful to assess the applicability of the [^{18}F]MPPF microPET strategy for quantifying 5-HT$_{1A}$R binding in the brain of living rats and its reliability over time, notably in an anatomical region as small as the DRN.

Materials and methods

Animals

All procedures involving animals and their care were conducted in strict accordance with the Guidelines for Care of Laboratory Animals of the French Ministère de l'Agriculture et de la Forêt (87–848) and the European Economic Community (86–60, EEC) and the Guide to the Care and Use of Experimental Animals (Ed2) of the Canadian Council on Animal Care. The magnetic resonance imaging (MRI) protocol was approved by the Ethics Committee of the Centre Léon Bérard (Lyon, France) and the microPET imaging protocol by the McGill University Animal Care Committee (Montreal, QC, Canada).

MRI data were obtained from a single adult male, Sprague–Dawley rat (Élevage Dépré, Saint Doulchard, France) weighing 250 g. The microPET experiments were carried out in 13 adult male, Sprague–Dawley rats (Charles River, St-Constant, QC, Canada) weighing 250±25 g. These rats were housed individually at a constant temperature (20–22°C) and under a 12-h light/dark cycle, with free access to food and water.

Magnetic resonance imaging

The MRI study was carried out on a 7-T Bruker BioSpin system (Bruker Biospin, Ettlingen, Germany) using a surface coil of 23 mm in diameter. After anaesthesia by inhalation of isoflurane (5% for 2 min followed by 2%) in air (2 L/min), the rat was placed in a heated mat-cushioned body holder (37°C), with its head immobilised by a hard palate piece. The MRI acquisition (BIO 7T, Bruker BioSpin MRI GmbH, resolution) consisted of a 3D anatomical scan of 38-min duration. A 22.5×20×22.5-mm field of view (FOV) was used to obtain a 256×128 matrix divided in 45 slices, with a resolution of 88×156×500 μm.

MicroPET scans

[^{18}F]MPPF was obtained by nucleophilic fluoration of a nitro precursor as previously described in detail [20]. The

radiochemical yield was in the order of 20–25% at the end of synthesis, with a specific activity of 37–111 GBq/μmol.

MicroPET imaging of [^{18}F]MPPF was performed with a MicroPET R4 (Siemens Preclinical Solutions, Knoxville, TN, USA) scanner, which has a volumetric resolution better than 15.6 μl within 20 mm of the centre of the FOV [28]. The spatial resolution of this scanner at the centre of the FOV is 1.85 mm full-width at half-maximum (FWHM) in the axial direction and 1.66 mm FWHM in the transaxial and tangential directions.

After isoflurane anaesthesia as above, the rat was placed in the body holder with its head affixed to the incisor bar. The laser guidance system at the front of the gantry was used to centre the brain in the FOV. A 10-min transmission scan was acquired using a rotating ^{57}Co point source, followed by a bolus injection of 7.4–11.1 MBq of [^{18}F]MPPF in the tail vein. Radioactivity was then measured in 27 sequential time frames of increasing duration (8×30, 6×60, 5×120 and 8×300 s) for a total duration of 60 min.

Sinograms were normalised, corrected for randoms, scatter, attenuation, dead time and radio element decay and finally reconstructed with a filtered backprojection (Hanning filter of cut-off 0.5 cycles/pixels). This allowed the dynamic study of 18 volumes, each with a 128×128 matrix divided in 63 slices and 0.6 mm^3 in voxel size.

Analysis of microPET data

Dynamic PET volumes from 0 to 60 min were integrated and manually co-registered with MRI data (Register-1.3.6 and Minc-2.0.9, MNI-BIC Software, Montreal, Canada) using a rigid body transformation with 6 degrees of freedom. The obtained transformation matrix was then applied to the dynamic PET volumes. A 20-mm^3 ellipse was drawn in the centre of the caudal area of cerebellum on the co-registered MRI (Display-1.3, MNI-BIC Software).

This allowed us to estimate the binding parameters of the tracer according to the simplified reference tissue model (SRTM), as previously applied to [^{11}C]WAY100635 [29] and to [^{18}F]MPPF in humans [30, 31] and very recently to [^{18}F]MPPF in rats [32]. The SRTM is based on the analytic solution of the compartment model for estimating three parameters without the use of an arterial sampling input function. In this model, BP is the ratio of available receptor density to receptor affinity, with BP $\approx B'_{\max}/K'_{\mathrm{d}}$ ($B'_{\max}$ being the apparent $B_{\max}$ and K'_{d} the apparent dissociation constant), k_2 is the tracer's efflux between the vascular system and R_1 is the ratio of plasma to brain transport constant in the volume of interest (VOI) and reference region (K_1/K'_1). The cerebellum was used as the region of reference since it contains very few 5-HT$_{1A}$R in adult rat [33, 34].

Parametric images of BP, k_2 and R_1 were calculated from individual voxel time–activity curves using Receptor Parametric Mapping software [35]. BP volumes were automatically co-registered using PET-to-PET cross-correlation with 7 degrees of freedom (mni_autoreg-0.99.3, MNI-BIC Software). The same transformation matrices were applied to parametric images of k_2 and R_1. All 18 PET volumes of BP were averaged into a single volume, which was then fused with the MRI to draw the regions containing BP and regrouped into anatomical VOIs (Display-1.3, MNI-BIC Software). The Paxinos and Watson's stereotaxic atlas of the rat brain [36] was used as an anatomical reference to identify eight regions on this MRI and draw the corresponding VOIs for medial prefrontal cortex (27 mm^3), septum (8 mm^3), hippocampus (100 mm^3), raphe nuclei (3 mm^3), entorhinal cortex (15 mm^3), amygdala (7 mm^3), paraventricular hypothalamic nucleus (4 mm^3) and raphe obscurus (2 mm^3). Regional radioactivity concentration (kilobecquerel per cubic centimetre) was also measured in the dynamic PET volumes for each VOI and plotted versus time.

Test–retest variability (Eq. 1), intraclass correlation coefficient (Eq. 2) and the coefficient of variation (Eq. 3) were computed with the following equations:

$$\text{Test}-\text{retest variability(TRV)} = 100 \cdot \frac{|\text{scan}_1 - \text{scan}_2|}{(\text{scan}_1 - \text{scan}_2)/2} \quad (1)$$

$$\text{Intraclass correlation coefficient(ICC)} = \frac{\text{MSBS} - \text{MSWS}}{\text{MSBS} + (n-1)\text{MSWS}} \quad (2)$$

$$\text{Coefficient of variation(CV)} = 100 \cdot \frac{\sigma}{\mu} \quad (3)$$

MSBS and MSWS are the mean sum of squares between and within subjects, respectively; n is the number of within-subject measurements, μ is the mean value and σ is the standard deviation. ICC represents the ratio of between-subject variance to total variance and is the appropriate metric for assessing within-subject reliability. Therefore, ICC values will be particularly high when within-subject (i.e. within-subject between-session) variance is low and between-subject variance is high. CV is a measure of dispersion and often referred to as the relative standard deviation. Regional BP values were checked for normality using d'Agostino and Pearson's omnibus normality test and then compared by one-way ANOVA with Bonferroni's post test.

Student's two-tailed paired t test was also used to assess regional differences in BP between test and retest scans (GraphPad Prism version 5, GraphPad Software, San Diego, CA, USA).

Statistical parametric mapping (SPM) analysis

Co-registered parametric images of BP were smoothed with a 1-mm Gaussian blur, and a voxelwise paired t test was performed in SPM5 (Wellcome Trust Centre for Neuroimaging at UCL, UK) to examine differences between test and retest scans (voxel size 0.1×0.2×0.5 mm; 1,474,560 voxels; height threshold T=7.17, p<0.001 uncorrected; extent threshold k=10 voxels, p=0.031).

Pretreatment with 5-HT_{1A} receptor agonist

A single rat was injected with a saline solution containing the 5-HT_{1A} agonist 8-OH-DPAT (5 mg/kg, i.p.; Sigma-Aldrich, Oakville, Ontario, Canada) 60 min before undergoing a [^{18}F]MPPF microPET scan.

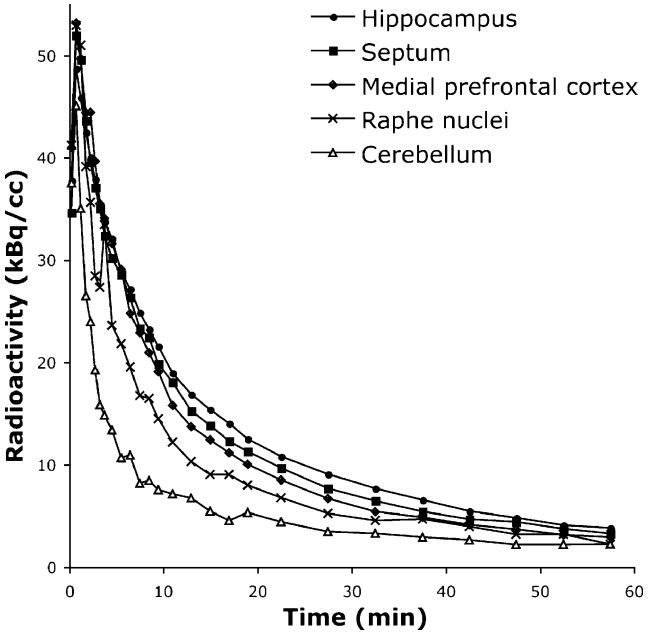

Fig. 1 Regional radioactivity in the hippocampus, septum, medial prefrontal cortex, raphe nuclei and cerebellum after the bolus injection of [^{18}F]MPPF. Mean from 18 scans in 12 rats, including the test–retest in six of these rats

Results

As previously observed in PET studies in cat [26, 37] and human (reviewed in [23]), the regional radioactivity time curves after i.v. injection in the rat indicated an initial surge of [^{18}F]MPPF throughout brain, followed within minutes by a relatively rapid washout over the next hour, but at varying rates according to the region examined (Fig. 1). At all time points, the highest radioactivity was that measured in the hippocampus, followed by septum, medial prefrontal cortex and raphe nuclei. The radioactivity in cerebellum dropped sharply in the first 5 min after the bolus injection of [^{18}F]MPPF and remained low at all time points thereafter (Fig. 1).

Receptor parametric mapping revealed the presence of specific 5-HT_{1A} BP in the medial prefrontal cortex, septum, amygdala, hippocampus, entorhinal cortex, raphe nuclei, paraventricular hypothalamic nucleus and raphe obscurus (Figs. 2 and 3). The co-registration of BP and MRI images confirmed the raphe nuclei as the origin of [^{18}F]MPPF binding in mesencephalon, which was clearly discernible and easily delineated from its immediate surround in the coronal (Fig. 2) as well as sagittal and horizontal planes (Fig. 3).

As measured with the SRTM (Table 1), the highest BP value was that in hippocampus (1.10±0.20), followed by entorhinal (1.09±0.28), septum (1.08±0.19), medial prefrontal cortex (1.00±0.16), amygdala (0.84±0.11), DRN (0.58±0.11), paraventricular hypothalamic nucleus (0.53±0.14) and raphe obscurus (0.52±0.16). The comparison of regional BP values indicated that most of the regions examined were significantly different from one another as shown in Fig. 4.

The estimated regional values of k_2 ranged from 0.010±0.005 in the raphe obscurus to 0.015±0.002 in the medial prefrontal cortex (Table 1). Regional differences in k_2 were only found in the medial prefrontal cortex, which differed significantly from the entorhinal cortex (p<0.05) and raphe obscurus (p<0.01; Fig. 4).

Regional R_1 values ranged from 0.70±0.13 in the amygdala to 0.96±0.22 in the DRN (Table 1). They differed significantly in DRN not only from those measured in the septum (p<0.05) and amygdala (p<0.001) but also between the latter region and raphe obscurus (p<0.01; Fig. 2).

As shown in Table 2, the average percent changes between test and retest BP values ranged from 0.3% in the basolateral amygdaloid nucleus to 10.2% in the DRN, while BP test–retest variability ranged from 7% in hippocampus to 34% in the raphe obscurus. ICC values ranged from to −0.06 in the amygdala to 0.92 in the entorhinal cortex. The test–retest variability in DRN (18%) was comparable to that in the paraventricular hypothalamic nucleus (17%). There were no statistically significant differences between test and retest BP values when compared by Student's paired t test in the VOIs

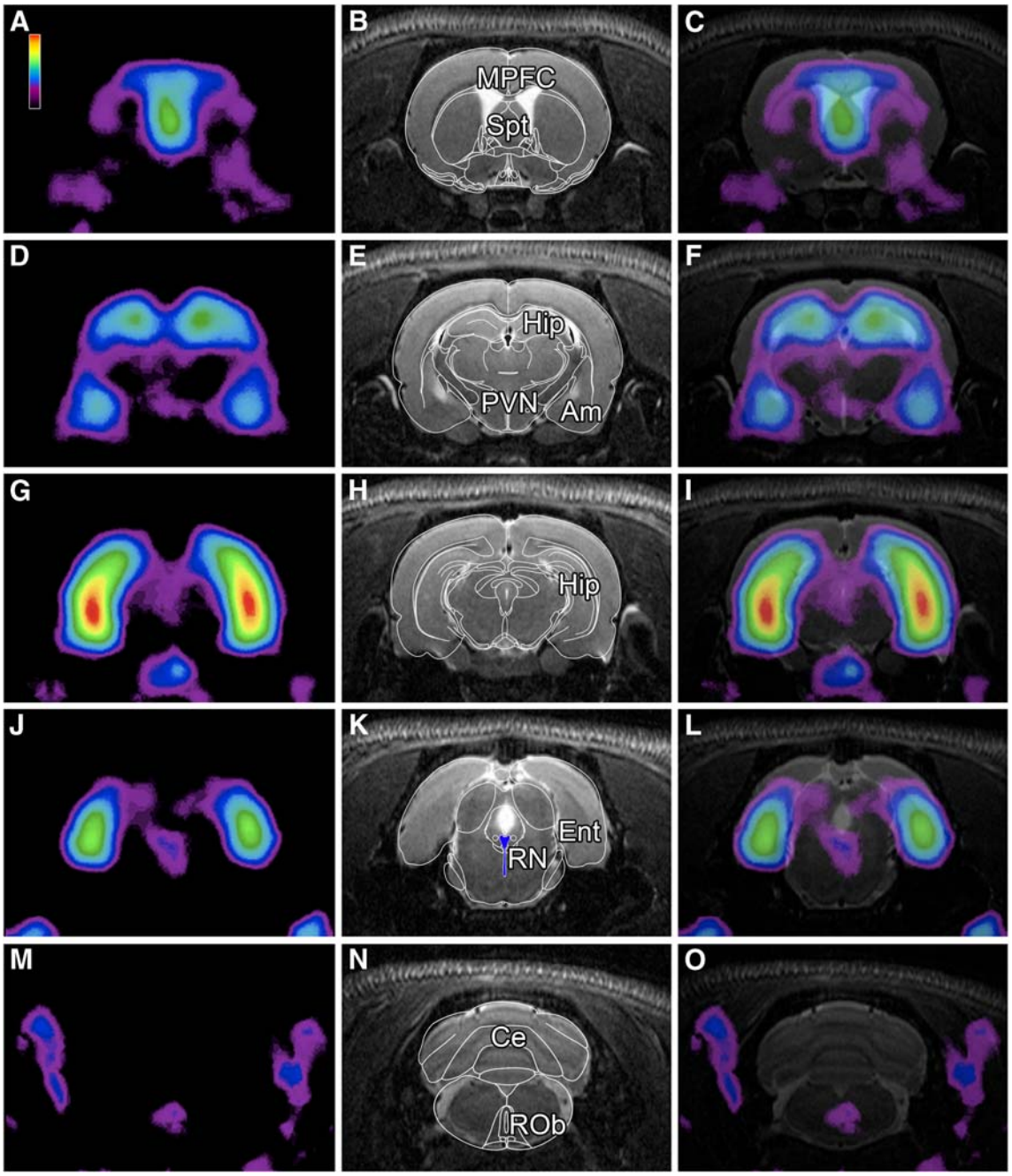

Fig. 2 Pseudo-colour visualisation of [^{18}F]MPPF BP (**a**, **d**, **g**, **j**, **m**), MRI views (**b**, **e**, **h**, **k**, **n**) and fusion of both type of images (**c**, **f**, **i**, **l**, **o**) at different coronal levels across rat brain. Data from 18 microPET scans in 12 rats and one MRI, as described in the "Materials and methods". In **b**, **e**, **h** and **n**, diagrams from Paxinos and Watson's atlas of the rat brain [36] are superposed on the MRI images to identify regions of interest. *MPFC* Medial prefrontal cortex, *Spt* septum, *PVN* paraventricular hypothalamic nucleus, *Am* amygdala, *Hip* hippocampus, *RN* raphe nuclei, *Ent* entorhinal cortex, *Ce* cerebellum, *ROb*, raphe obscurus. Pseudo-colour scale: BP 0.3–2

(Table 2) or by voxelwise analysis with SPM (data not shown).

Pretreatment with the 5-HT$_{1A}$ agonist 8-OH-DPAT completely blocked the binding of [^{18}F]MPPF in all cerebral regions (data not shown).

Discussion

The radioactivity curves here obtained from five regions of rat brain, in the hour following the bolus injection of [^{18}F]MPPF, were comparable to those previously measured with

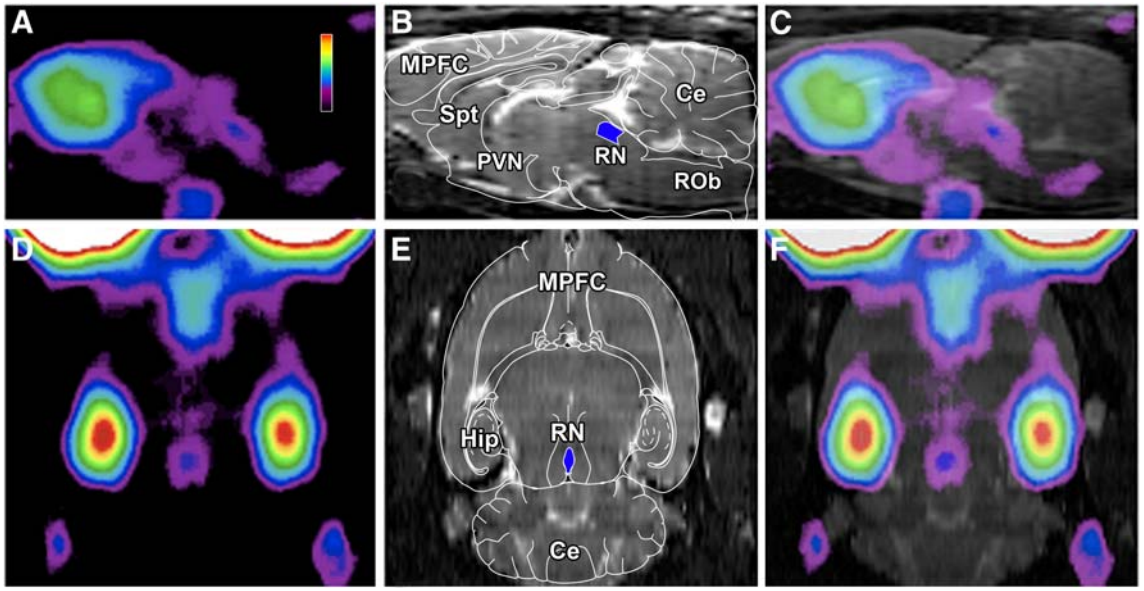

Fig. 3 Pseudo-colour visualisation of [^{18}F]MPPF BP (**a**, **d**), MRI views (**b**, **e**) and fusion of both types of images (**c**, **f**) as in Fig. 2, but in the sagittal (**a**, **b**, **c**) and the horizontal (**d**, **e**, **f**) planes. *MPFC* Medial prefrontal cortex, *Spt*, septum, *PVN* paraventricular hypothalamic nucleus, *Hip* hippocampus, *RN* raphe nuclei, *Ce* cerebellum, *ROb* raphe obscurus. Pseudo-colour scale: BP 0.3–2

PET in rats [21], cats [20, 26, 37, 38], non-human primates [21, 39] and humans [30, 40–42]. The hippocampus displayed the highest radioactivity, followed by septum, medial prefrontal cortex and raphe nuclei. A similar distribution pattern has also been reported using in vitro [19, 33, 43, 44] or ex vivo [45, 46] autoradiography to measure the density of radioligand binding to 5-HT$_{1A}$R in rat brain. Furthermore, the specificity of [^{18}F]MPPF binding was confirmed by the pretreatment with 8-OH-DPAT, which completely blocked [^{18}F]MPPF binding in every brain region containing 5-HT$_{1A}$ receptors.

The present report provides regional estimates of [^{18}F]MPPF BP, k_2 and R_1 values for rat brain. As shown in Table 3, the BP values were in the same range as those previously reported in various species using PET. Very recently, Millet et al. [32] have reported strikingly similar [^{18}F]MPPF BP values in the hippocampus and raphe nuclei of rats using the YAP-(S)PET scanner, even though their data were not corrected for attenuation or scatter.

The realignment procedure used in the determination of PET volumes, as described in the "Materials and methods", was crucial in obtaining reliable measurements from the various regions examined (see [47]). In this way, a single template could be used to extract BP, k_2 and R_1 values from each volume, thus reducing the risk of a sampling bias associated with the drawing of ROIs. This method allowed us to estimate BP in regions that are not commonly sampled in microPET studies, such as the septum, PVN, amygdala, DRN and even smaller regions such as the raphe obscurus (Robs).

Despite our best efforts, however, a number of methodological constraints could not be avoided. Foremost, in view of the limited resolution of the microPET camera and the size of the smaller regions examined (raphe nuclei, PVN, RObs), it was likely that the BP values in these regions were underestimated due to partial volume effects, as previously noted with [^{11}C]WAY-100635 in human NRD [29, 48]. This underestimation might have been less with [^{18}F]MPPF than [^{11}C]WAY-100635 because of the lower energy of the ^{18}F radionuclide, yet significant. On the other hand, a potential source of overestimation was the accumulation of radioactivity in the Harderian glands, located behind the eyes (visible in Figs. 2 and 3), which could have increased readings from adjacent regions such as the medial prefrontal cortex. It should also be noted that anaesthetics may affect the binding of radioligands to 5-HT$_{1A}$R by modulating the affinity state of G-protein-coupled receptors [49], as convincingly shown to be the case for dopamine receptors [50, 51].

Nevertheless, the reproducibility and reliability of our sampling method was evidenced by a relatively low variability in repeated measurements of BP and high ICC, at least in the larger brain regions examined (see Table 2). The regional values of test–retest variability were generally lower than those reported with [^{11}C]WAY-100635 in humans (e.g. hippocampus 26±21%, [48]), but on par with those found with [^{18}F]MPPF in cats (e.g. hippocampus 7±6%, [26]) and humans (e.g. hippocampus

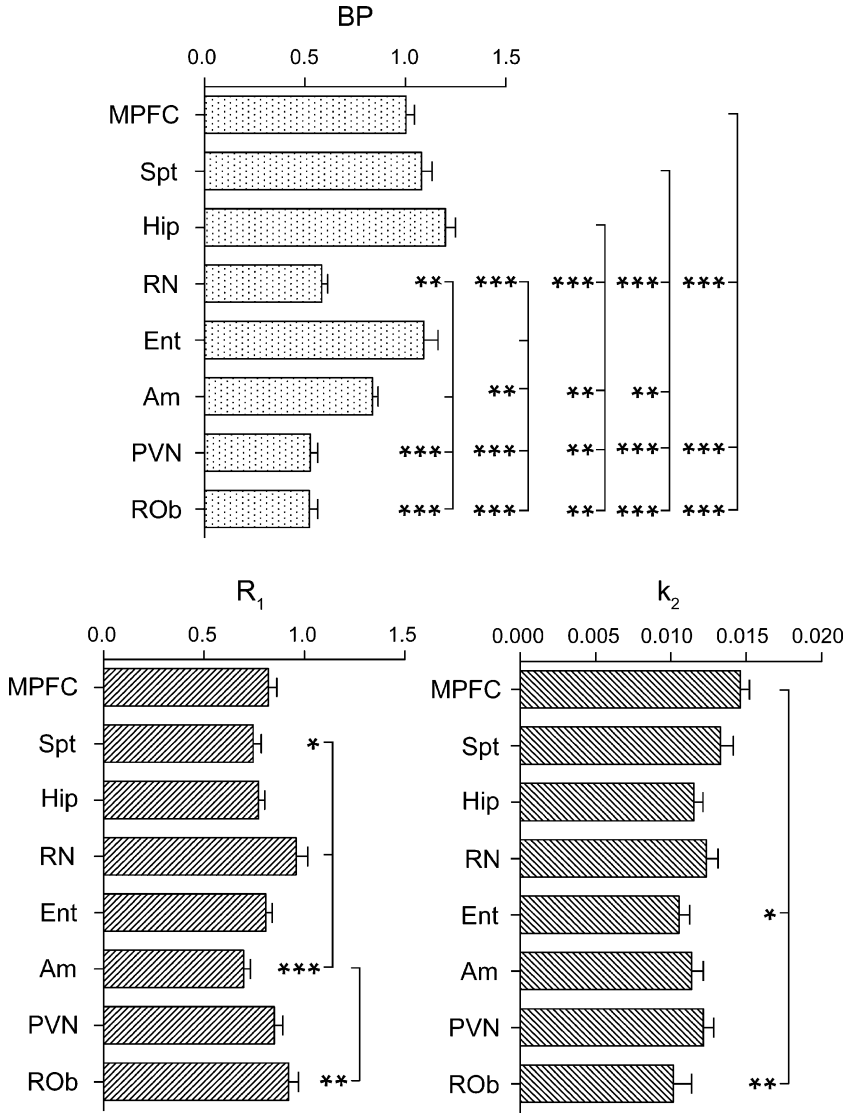

Fig. 4 Regional values of BP, R_1 and k_2. Data from 18 microPET scans, as described in the "Materials and methods". Regions showing statistically significant differences are linked by *hooks with asterisks* in front of the differing region(s). *$p<0.05$, **$p<0.01$ and ***$p<0.001$ by one-way ANOVA with Bonferroni's post test. *MPFC* Medial prefrontal cortex, *Spt* septum, *Hip* hippocampus, *RN* raphe nuclei, *Ent* entorhinal cortex, *Am* amygdala, *PVN* paraventricular hypothalamic nucleus, *ROb* raphe obscurus

7±3%, [31]; e.g. hippocampus 11±11%, [27]). In the hippocampus, [^{18}F]MPPF BP test–retest variability was in the same range as those reported with [^{11}C]raclopride (14.0%) and [^{18}F]FECT (7.7%) in rat striatum [47]. These values were also comparable to the test–retest variability of DVR measured with [^{11}C]raclopride (8.3%) in rat striatum [52]. Test–retest variability was typically higher (and ICC lower) in smaller brain regions. This was particularly noticeable in the RObs. In fact, it was not expected to even be able to identify such a small anatomical region as a site of [^{18}F]MPPF binding, in view of the resolution and sensitivity of the microPET scanner. The low ICC values found in certain regions could also reflect the fact that intersubject variability is relatively low in rats as opposed to human subjects [53]. This could imply that, in [^{18}F]MPPF microPET studies involving repeated scans, it might not be indispensable to use the same animal as its own control.

MicroPET imaging of 5-HT$_{1A}$ receptors with [^{18}F]MPPF represents a valuable asset to study the activation of 5-HT$_{1A}$ brain receptors in vivo. Pharmacological compounds, which bind to 5-HT$_{1A}$ with high affinity, occupy 5-HT$_{1A}$ receptor binding sites and/or displace [^{18}F]MPPF binding, as we have observed with WAY-100635 in cats (unpublished data) and 8-OH-DPAT in rats. The use of this technique might help to determine whether atypical antipsychotics with low affinity for 5-HT$_{1A}$ receptors in vitro actually interact with 5-HT$_{1A}$ heteroreceptors in vivo [54, 55] and also to better characterise the activation and internalisation of 5-HT$_{1A}$ autoreceptors by agonists [25, 56], SSRIs [24, 26, 27, 57] and atypical antipsychotics [58].

Table 1 [^{18}F]MPPF BP (binding potential), k_2 (tracer's efflux in the vascular system) and R_1 (ratio of plasma to brain transport constant) were measured with the simplified reference tissue model (SRTM), as described in the "Materials and methods"

Mean±SD from 18 scans in 12 rats, including the test–retest in six of these rats

Region	BP (mean±SD)	k_2 (mean±SD)	R_1 (mean±SD)
Medial prefrontal cortex	1.00±0.16	0.015±0.002	0.82±0.16
Septum	1.08±0.20	0.013±0.003	0.75±0.15
Paraventricular hypothalamic nucleus	0.53±0.14	0.012±0.003	0.85±0.16
Amygdala	0.84±0.11	0.011±0.003	0.70±0.13
Hippocampus	1.20±0.19	0.012±0.002	0.77±0.12
Entorhinal cortex	1.09±0.28	0.011±0.003	0.81±0.12
Raphe nuclei	0.58±0.11	0.012±0.003	0.96±0.22
Nucleus raphe obscurus	0.52±0.16	0.010±0.005	0.92±0.19

Table 2 Coefficient of variation (CV), test–retest variability (TRV) and intraclass correlation coefficient (ICC) were computed, as described in the "Materials and methods"

Region	BP test (mean±SD)	CV (%)	BP retest (mean±SD)	CV (%)	Mean change (|%|)	TRV (%±SD)	*t* test (*p*)	ICC
Medial prefrontal cortex	0.95±0.14	14.6	1.03±0.06	6.2	8.5	9.7±10.3	0.16	0.54
Septum	1.11±0.11	10.2	1.05±0.16	15.5	5.5	13.3±9.9	0.51	0.29
Paraventricular hypothalamic nucleus	0.50±0.09	17.8	0.51±0.03	6.0	1.7	17.3±7.8	0.86	0.07
Amygdala	0.81±0.10	13.0	0.81±0.08	9.5	0.3	15.0±8.9	0.97	−0.06
Hippocampus	1.10±0.17	15.6	1.08±0.13	11.9	2.4	11.7±6.0	0.71	0.67
Entorhinal cortex	1.08±0.17	16.1	1.10±0.17	15.4	2.6	6.9±4.2	0.48	0.92
Raphe nuclei	0.52±0.08	14.6	0.57±0.09	15.3	10.2	18.4±5.5	0.29	0.41
Nucleus raphe obscurus	0.48±0.12	24.7	0.46±0.14	30.6	2.6	34.5±23.7	0.89	0.22

Means±SD from six rats (two scans per rat)

Table 3 5-HT$_{1A}$ BP values in selected PET studies

Study Radioligand Species	Present [^{18}F]MPPF Rat	[32] [^{18}F]MPPF Rat	[59] [^{11}C]RWAY Rat	[26] [^{18}F]MPPF Cat	[60] [^{18}F]PWAY Monkey	[31] [^{18}F]MPPF Human	[27] [^{18}F]MPPF Human
Region							
Prefrontal cortex	1±0.2	–	1.2±0.1	1.1±0.1	1.9±0.1	0.8±0.1	0.7±0.2
Septum	1.1±0.2	–	–	1.4±0.1	–	–	–
Hippocampus	1.2±0.2	0.9±0.5	1.5±0.2	1.5±0.2	–	1.4±0.2	1.7±0.5
Entorhinal cortex	1.1±0.2	–	–	–	–	1.3±0.2	–
Raphe nuclei	0.5±0.1	0.5±0.4	–	0.6±0.1	0.5±0.1	0.3±0.1	0.6±0.2

Acknowledgments The authors are grateful to Shadreck Mzengeza for his help with the radiochemistry. The work was funded by the Canadian Institutes for Health Research (operating grants to C.B. and L.D.). N.A. held a postdoctoral fellowship, and L.D. benefitted from an infrastructure grant from the Fonds de la Recherche en Santé du Québec.

Conflict of interest The authors declare that they have no competing financial interests.

References

1. Lucki I. The spectrum of behaviors influenced by serotonin. Biol Psychiatry 1998;44:151–62.
2. Frazer AHJ. Serotonin. Philadelphia: Lippincott-Raven; 1999.
3. Dahlström A, Fuxe K. Evidence for the existence of monoamine-containing neurons in the central nervous system. I. Demonstration of monoamines in the cell bodies of brain stem neurons. Acta Physiol Scand Suppl. 1964;232:231–55.
4. Ungerstedt U. Stereotaxic mapping of the monoamine pathways in the rat brain. Acta Physiol Scand Suppl. 1971;367:1–48.
5. Moore RY, Halaris AE, Jones BE. Serotonin neurons of the midbrain raphe: ascending projections. J Comp Neurol. 1978;180:417–38.
6. Parent A, Descarries L, Beaudet A. Organization of ascending serotonin systems in the adult rat brain. A radioautographic study after intraventricular administration of [^{3}H]5-hydroxytryptamine. Neuroscience 1981;6:115–38.
7. Steinbusch HW. Distribution of serotonin-immunoreactivity in the central nervous system of the rat-cell bodies and terminals. Neuroscience 1981;6:557–618.
8. Hornung JP. The human raphe nuclei and the serotonergic system. J Chem Neuroanat. 2003;26:331–43.
9. Roth B. The serotonin receptors: from molecular pharmacology to human therapeutics. Totowa: Humana; 2006.
10. Lanfumey L, Hamon M. 5-HT1 receptors. Curr Drug Targets CNS Neurol Disord. 2004;3:1–10.
11. Jones BJ, Blackburn TP. The medical benefit of 5-HT research. Pharmacol Biochem Behav. 2002;71:555–68.
12. Hensler JG. Regulation of 5-HT1A receptor function in brain following agonist or antidepressant administration. Life Sci. 2003;72:1665–82.
13. Piñeyro G, Blier P. Autoregulation of serotonin neurons: role in antidepressant drug action. Pharmacol Rev. 1999;51:533–91.
14. Haddjeri N, Blier P, de Montigny C. Long-term antidepressant treatments result in a tonic activation of forebrain 5-HT1A receptors. J Neurosci. 1998;18:10150–6.
15. Shen C, Li H, Meller E. Repeated treatment with antidepressants differentially alters 5-HT1A agonist-stimulated [^{35}S]GTP gamma S binding in rat brain regions. Neuropharmacology 2002;42:1031–8.
16. Elena Castro M, Diaz A, del Olmo E, Pazos A. Chronic fluoxetine induces opposite changes in G protein coupling at pre and postsynaptic 5-HT1A receptors in rat brain. Neuropharmacology 2003;44:93–101.
17. Castro E, Tordera RM, Hughes ZA, Pei Q, Sharp T. Use of Arc expression as a molecular marker of increased postsynaptic 5-HT function after SSRI/5-HT1A receptor antagonist co-administration. J Neurochem. 2003;85:1480–7.
18. El Mansari M, Sanchez C, Chouvet G, Renaud B, Haddjeri N. Effects of acute and long-term administration of escitalopram and citalopram on serotonin neurotransmission: an in vivo electrophysiological study in rat brain. Neuropsychopharmacology 2005;30:1269–77.
19. Shiue CY, Shiue GG, Mozley PD, Kung MP, Zhuang ZP, Kim HJ, et al. P-[^{18}F]-MPPF: a potential radioligand for PET studies of 5-HT1A receptors in humans. Synapse 1997;25:147–54.
20. Le Bars D, Lemaire C, Ginovart N, Plenevaux A, Aerts J, Brihaye C, et al. High-yield radiosynthesis and preliminary in vivo evaluation of p-[^{18}F]MPPF, a fluoro analog of WAY-100635. Nucl Med Biol. 1998;25:343–50.
21. Plenevaux A, Weissmann D, Aerts J, Lemaire C, Brihaye C, Degueldre C, et al. Tissue distribution, autoradiography, and metabolism of 4-(2¢-methoxyphenyl)-1-[2′ -[N-2′-pyridinyl)-p-[(18)F]fluorobenzamido]ethyl]piperazine (p-[(18)F]MPPF), a new serotonin 5-HT(1A) antagonist for positron emission tomography: an in vivo study in rats. J Neurochem. 2000;75:803–11.
22. Zimmer L, Pain F, Mauger G, Plenevaux A, Le Bars D, Mastrippolito R, et al. The potential of the beta-Microprobe, an intracerebral radiosensitive probe, to monitor the [(18)F]MPPF binding in the rat dorsal raphe nucleus. Eur J Nucl Med Mol Imaging. 2002;29:1237–47.
23. Aznavour N, Zimmer L. [^{18}F]MPPF as a tool for the in vivo imaging of 5-HT1A receptors in animal and human brain. Neuropharmacology 2007;52:695–707.
24. Riad M, Zimmer L, Rbah L, Watkins KC, Hamon M, Descarries L. Acute treatment with the antidepressant fluoxetine internalizes 5-HT1A autoreceptors and reduces the in vivo binding of the PET radioligand [^{18}F]MPPF in the nucleus raphe dorsalis of rat. J Neurosci. 2004;24:5420–6.
25. Zimmer L, Riad M, Rbah L, et al. Toward brain imaging of serotonin 5-HT1A autoreceptor internalization. NeuroImage 2004;22:1421–6.
26. Aznavour N, Rbah L, Riad M, Reilhac A, Costes N, Descarries L, et al. A PET imaging study of 5-HT(1A) receptors in cat brain after acute and chronic fluoxetine treatment. NeuroImage 2006;33:834–42.
27. Sibon I, Benkelfat C, Gravel P, Aznavour N, Costes N, Mzengeza S, et al. Decreased [(18)F]MPPF binding potential in the dorsal raphe nucleus after a single oral dose of fluoxetine: a positron-emission tomography study in healthy volunteers. Biol Psychiatry. 2008;63:1135–40.
28. Knoess C, Siegel S, Smith A, Newport D, Richerzhagen N, Winkeler A, et al. Performance evaluation of the microPET R4 PET scanner for rodents. Eur J Nucl Med Mol Imaging. 2003;30:737–47.
29. Gunn RN, Sargent PA, Bench CJ, Rabiner EA, Osman S, Pike VW, et al. Tracer kinetic modeling of the 5-HT1A receptor ligand [carbonyl-^{11}C]WAY-100635 for PET. NeuroImage 1998;8:426–40.
30. Costes N, Merlet I, Zimmer L, Lavenne F, Cinotti L, Delforge J, et al. Modeling [^{18}F]MPPF positron emission tomography kinetics for the determination of 5-hydroxytryptamine(1A) receptor concentration with multiinjection. J Cereb Blood Flow Metab. 2002;22:753–65.
31. Costes N, Zimmer L, Reilhac A, Lavenne F, Ryvlin P, Le Bars D. Test–retest reproducibility of ^{18}F-MPPF PET in healthy humans: a reliability study. J Nucl Med. 2007;48:1279–88.
32. Millet P, Moulin M, Bartoli A, Del Guerra A, Ginovart N, Lemoucheux L, et al. In vivo quantification of 5-HT(1A)-[(18)F]MPPF interactions in rats using the YAP-(S)PET scanner and a beta-microprobe. NeuroImage 2008;41:823–34.
33. Pazos A, Palacios JM. Quantitative autoradiographic mapping of serotonin receptors in the rat brain. I. Serotonin-1 receptors. Brain Res. 1985;346:205–30.
34. El Mestikawy S, Riad M, Laporte AM, Vergé D, Daval G, Gozlan H, et al. Production of specific anti-rat 5-HT1A receptor antibodies in rabbits injected with a synthetic peptide. Neurosci Lett. 1990;118:189–92.
35. Gunn RN, Lammertsma AA, Hume SP, Cunningham VJ. Parametric imaging of ligand-receptor binding in PET using a simplified reference region model. NeuroImage 1997;6:279–87.

36. Paxinos G, Watson C. The rat brain in stereotaxic coordinates. 4th ed. New York: Academic; 1998.
37. Aznavour N, Rbah L, Leger L, Buda C, Sastre JP, Imhof A, et al. A comparison of in vivo and in vitro neuroimaging of 5-HT1A receptor binding sites in the cat brain. J Chem Neuroanat. 2006;31:226–32.
38. Ginovart N, Hassoun W, Le Bars D, Weissmann D, Leviel V. In vivo characterization of p-[(18)F]MPPF, a fluoro analog of WAY-100635 for visualization of 5-HT(1a) receptors. Synapse 2000;35:192–200.
39. Shively CA, Friedman DP, Gage HD, Bounds MC, Brown-Proctor C, Blair JB, et al. Behavioral depression and positron emission tomography-determined serotonin 1A receptor binding potential in cynomolgus monkeys. Arch Gen Psychiatry. 2006;63:396–403.
40. Passchier J, van Waarde A. Visualisation of serotonin-1A (5-HT1A) receptors in the central nervous system. Eur J Nucl Med. 2001;28:113–29.
41. Passchier J, van Waarde A, Pieterman RM, Elsinga PH, Pruim J, Hendrikse HN, et al. In vivo delineation of 5-HT1A receptors in human brain with [^{18}F]MPPF. J Nucl Med. 2000;41:1830–5.
42. Passchier J, van Waarde A, Pieterman RM, Elsinga PH, Pruim J, Hendrikse HN, et al. Quantitative imaging of 5-HT(1A) receptor binding in healthy volunteers with [(18)f]p-MPPF. Nucl Med Biol. 2000;27:473–6.
43. Khawaja X. Quantitative autoradiographic characterisation of the binding of [^{3}H]WAY-100635, a selective 5-HT1A receptor antagonist. Brain Res. 1995;673:217–25.
44. Gozlan H, Thibault S, Laporte AM, Lima L, Hamon M. The selective 5-HT1A antagonist radioligand [^{3}H]WAY 100635 labels both G-protein-coupled and free 5-HT1A receptors in rat brain membranes. Eur J Pharmacol. 1995;288:173–86.
45. Udo de Haes JI, Cremers TI, Bosker FJ, Postema F, Tiemersma-Wegman TD, den Boer JA. Effect of increased serotonin levels on [^{18}F]MPPF binding in rat brain: fenfluramine vs the combination of citalopram and ketanserin. Neuropsychopharmacology 2005; 30:1624–31.
46. Jagoda EM, Lang L, Tokugawa J, Simmons A, Ma Y, Contoreggi C, et al. Development of 5-HT1A receptor radioligands to determine receptor density and changes in endogenous 5-HT. Synapse 2006;59:330–41.
47. Casteels C, Vermaelen P, Nuyts J, Van Der Linden A, Baekelandt V, Mortelmans L, et al. Construction and evaluation of multitracer small-animal PET probabilistic atlases for voxel-based functional mapping of the rat brain. J Nucl Med. 2006;47:1858–66.
48. Parsey RV, Slifstein M, Hwang DR, Abi-Dargham A, Simpson N, Mawlawi O, et al. Validation and reproducibility of measurement of 5-HT1A receptor parameters with [carbonyl-^{11}C]WAY-100635 in humans: comparison of arterial and reference tissue input functions. J Cereb Blood Flow Metab. 2000;20:1111–33.
49. Seeman P, Kapur S. Anesthetics inhibit high-affinity states of dopamine D2 and other G-linked receptors. Synapse 2003;50:35–40.
50. Ginovart N, Wilson AA, Meyer JH, Hussey D, Houle S. [^{11}C]-DASB, a tool for in vivo measurement of SSRI-induced occupancy of the serotonin transporter: PET characterization and evaluation in cats. Synapse 2003;47:123–33.
51. Hassoun W, Le Cavorsin M, Ginovart N, Zimmer L, Gualda V, Bonnefoi F, et al. PET study of the [^{11}C]raclopride binding in the striatum of the awake cat: effects of anaesthetics and role of cerebral blood flow. Eur J Nucl Med Mol Imaging. 2003;30:141–8.
52. Alexoff DL, Vaska P, Marsteller D, Gerasimov T, Li J, Logan J, Fowler JS, et al. Reproducibility of ^{11}C-raclopride binding in the rat brain measured with the microPET R4: effects of scatter correction and tracer specific activity. J Nucl Med. 2003;44:815–22.
53. Costes N, Merlet I, Ostrowsky K, Faillenot I, Lavenne F, Zimmer L, et al. A 18F-MPPF PET normative database of 5-HT1A receptor binding in men and women over aging. J Nucl Med. 2005;46:1980–9.
54. Ichikawa J, Ishii H, Bonaccorso S, Fowler WL, O'Laughlin IA, Meltzer HY. 5-HT(2A) and D(2) receptor blockade increases cortical DA release via 5-HT(1A) receptor activation: a possible mechanism of atypical antipsychotic-induced cortical dopamine release. J Neurochem. 2001;76:1521–31.
55. Díaz-Mataix L, Scorza MC, Bortolozzi A, Toth M, Celada P, Artigas F. Involvement of 5-HT1A receptors in prefrontal cortex in the modulation of dopaminergic activity: role in atypical antipsychotic action. J Neurosci. 2005;25:10831–43.
56. Riad M, Watkins KC, Doucet E, Hamon M, Descarries L. Agonist-induced internalization of serotonin-1a receptors in the dorsal raphe nucleus (autoreceptors) but not hippocampus (heteroreceptors). J Neurosci. 2001;21:8378–86.
57. Riad M, Rbah L, Verdurand M, Aznavour N, Zimmer L, Descarries L. Unchanged density of 5-HT(1A) autoreceptors on the plasma membrane of nucleus raphe dorsalis neurons in rats chronically treated with fluoxetine. Neuroscience 2008;151: 692–700.
58. Heusler P, Newman-Tancredi A, Loock T, Cussac D. Antipsychotics differ in their ability to internalise human dopamine D2S and human serotonin 5-HT1A receptors in HEK293 cells. Eur J Pharmacol. 2008;581:37–46.
59. Liow JS, Lu S, McCarron JA, Hong J, Musachio JL, Pike VW, et al. Effect of a P-glycoprotein inhibitor, cyclosporin A, on the disposition in rodent brain and blood of the 5-HT1A receptor radioligand, [^{11}C](R)-(−)-RWAY. Synapse 2007;61:96–105.
60. Giovacchini G, Lang L, Ma Y, Herscovitch P, Eckelman WC, Carson RE. Differential effects of paroxetine on raphe and cortical 5-HT1A binding: a PET study in monkeys. NeuroImage 2005;28:238–48.